Original Article

Prototype edge-grown nanowire sensor array for the real-time monitoring and classification of multiple gases

Nguyen Xuan Thai [a], Nguyen Van Duy [a, *], Chu Manh Hung [a, **], Hugo Nguyen [b], Matteo Tonezzer [c, d], Nguyen Van Hieu [e, f], Nguyen Duc Hoa [a]

[a] International Training Institute for Materials Science (ITIMS), Hanoi University of Science and Technology (HUST), No. 1, Dai Co Viet, Hanoi, Viet Nam
[b] Uppsala University, Department of Materials Science and Engineering, Lägerhyddsvägen 1, 751 21, Uppsala, Sweden
[c] IMEM-CNR, sede di Trento - FBK, via alla Cascata 56/C, 38123, Povo, TN, Italy
[d] Università degli Studi di Trento, Via Calepina 14, 38122, Trento, Italy
[e] Electrical and Electronic Engineering, Phenikaa Institute for Advanced Study (PIAS), Phenikaa University, Yen Nghia, Ha Dong District, Hanoi, 10000, Viet Nam
[f] Phenikaa Research and Technology Institute (PRATI), A&A Green Phoenix Group, 167 Hoang Ngan, Hanoi, 10000, Viet Nam

ARTICLE INFO

ABSTRACT

The monitoring and classification of different gases using a single resistive semiconductor sensor are challenging because of the similar response characteristics. An array of separated sensors can be used as an electronic nose, but such arrays have a bulky structure and complex fabrication processes. Herein, we easily fabricated a gas-sensor array based on edge-grown SnO$_2$ nanowires for the real-time monitoring and classification of multiple gases. The array comprised four sensors and was designed on a glass substrate. SnO$_2$ nanowires were grown on-chip from the edge of electrodes, made contact together, and acted as sensing elements. This method was advantageous over the post-synthesis technique because the SnO$_2$ nanowires were directly grown from the edge of the electrodes rather than on the surface. Accordingly, damage to the electrode was avoided by alloying Sn with Pt at a high growth temperature. The sensing characteristics of the sensor array were further examined for different gases, including methanol, isopropanol, ethanol, ammonia, hydrogen sulphide and hydrogen. Radar plots were used to improve the selective detection of different gases and enable effective classification.

1. Introduction

The monitoring and classification of different gases are very important in various applications, including air quality monitoring, the food industry, and disease diagnosis (lung cancer, gastric cancer, asthma and chronic obstructive pulmonary disease) [1]. Conventionally, different gases can be classified through chromatography–mass spectrometry, but this technique is slow, bulky, and expensive [2]. Thus, simple, fast and real-time monitoring and classification of various gases using a single device is desirable [3]. A single device gas sensor is generally designed to monitor a specific gas, but in practical application, it is always

contaminated by interference [4]. The enhancement of the selectivity of a metal-oxide gas sensor [5] for application in monitoring a specific gas is challenging, because the behaviour of some reducing gases is similar when they adsorb on the surface of the sensing materials [6]. However, the selectivity, sensitivity, and speed of response and recovery of chemical sensors depend on the thermodynamics and kinetics of sensitive material/analyte interactions [7]. Therefore, selectivity toward an analyte such as gas can be enhanced by creating specific sensitive layers with novel metal decoration [8]. However, this process is limited to the detection of a specific gas. Sensor arrays have been developed for environmental monitoring, medicine and the food industry, because they can act as an electronic nose [9]. In principle, an array of sensors can be assembled from separately fabricated sensors made of different materials, but its structure is bulky and complex [10]. For example, Hwang et al. [11] used an array of resistive sensors based on enriched single-walled carbon nanotubes for the detection of tetrahydrocannabinol. Wang et al. [12] used molecularly modified Si nanowire field effect transistors in

* Corresponding author.
** Corresponding author.
E-mail addresses: nguyenvanduy@itims.edu.vn (N. Van Duy), mhchu@itims.edu.vn (C.M. Hung).
Peer review under responsibility of Vietnam National University, Hanoi.

combination with artificial sensing intelligence for the highly selective detection and identification of volatile organic compounds (VOCs). Multisensor systems are generally a combination of individual sensors [13–15]; they overcome some limitations, such as large size, high power consumption, and high cost [16]. Most of the recently reported electronic nose systems still use such a solution, with arrays of separate gas sensors mounted on a bulky carrier. This approach requires synthesis of separate, highly selective sensors, one for each analyte [17], which are then assembled into an array of sensors [10]. However, increasing the number of sensors to increase selectivity also increases the power consumption [18]. A single-chip sensor array is desirable for microsystem integration [19]. Two multisensor structures are suitable for integration, such as sensors that utilizes different gas-sensitive materials (or changing catalyst materials)) [20–22] and multisensor systems that use the same sensing material inside a working temperature gradient [23,24]. The use of different gas-sensitive materials on a chip in an array of sensors faces difficulties in the integration/deposition of sensing layers on the tiny chip; thus, the use of one sensing material has been reported [25,26], where a sensor was tested at different temperatures, and the sensing data were collected for gas analysis. In this report, a temperature gradient from 200 °C to 400 °C with an interval of 50 °C was realized using a programmable horizontal tube furnace as the test chamber. Multiple gases can be classified using multiple sensing channels, where each channel responds to several analytes [17,27]. A gradient microarray electronic nose based on percolating SnO_2 nanowires was developed for the classification of various gases by using the post-synthesis technique, where the nanowires were grown, collected, dispersed in solution and then spin-coated on the substrate before patterned deposition of the electrodes [28]. Another gradient microarray chip with dimensions of 3.5 mm × 3 mm was used as an alumina substrate material with an integrated heater on the back side. The gradient microarray was based on a single Pt-doped SnO_2 film subdivided into 16 gas sensor segments, which were coated by a gas permeable SiO_2-gradient membrane [29]. In these reports, the post-synthesis technique was applied, thus requiring a complex fabrication process. The development of an effective sensor array for the identification of different gases is difficult. Such a sensor array should be compact, easy to fabricate and of good sensing characteristics (fingerprint) for gas classification.

In this paper, the design, fabrication and testing of a single-chip sensor array is reported, based on a temperature gradient effect. The chip includes four sensors, each composed of SnO_2 nanowires grown from the edge of the Cr/Pt/Au/Pt/ITO (from bottom to top) thin film electrodes. The edge-grown nanowires are very homogenous and stable, without the damage of Pt metal by tin vapour during the thermal growth process. By simulation, we could design the sensor array with a temperature gradient that provides each sensor with different sensing signals to the same gas., We have also utilized radar plots to identify several gases in order to study the gas classification ability.

2. Experimental

2.1. Fabrication of microheater and electrodes

The design and simulation of the sensor array chip are shown in Fig. 1(a). The sensor array is composed of a microheater and four sensors. The fabricated sensor chip has six electrode pads, including two for the microheater and four for the sensors. Before fabricating, heat distribution was simulated on the designed structures using the software COMSOL Multiphysics to find the most suitable one. The heater and the sensor electrodes were made as sandwich
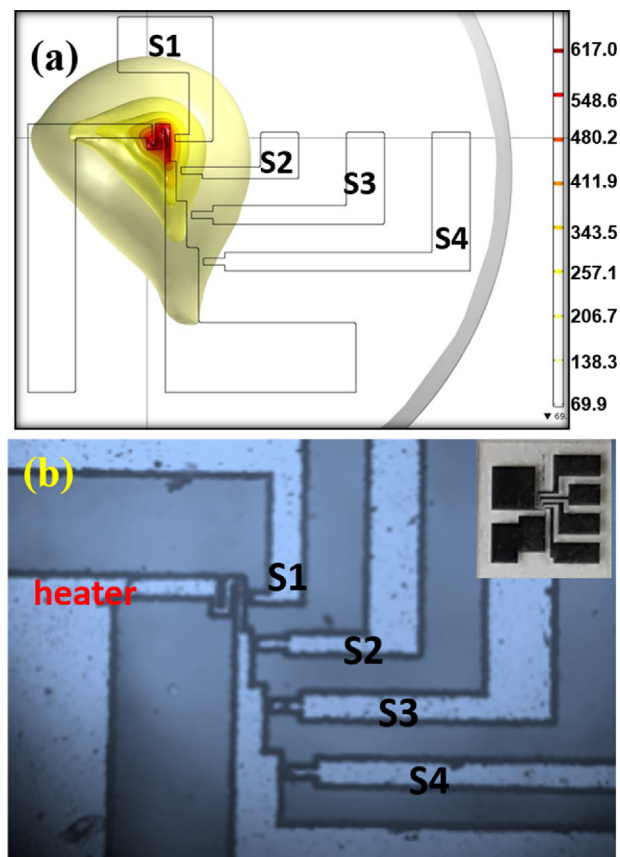

Fig. 1. Simulated image of heat distribution at the sensor centre region at the applied power of 165 mW (a); and the optical image of the fabricated sensor chip at the magnification of 100 with the inset of a whole chip (b).

structures of thin films from different layers of conducting material with thickness in the nanometre scale. To ease the meshing and computing step, we modelled the heater and the electrodes as single-layer elements of Pt with a thickness of 100 nm and resistance equivalent to the sandwich structures. Notably, the resistivities of the thin films in this simulation were set to room temperature, although they were subject to change with temperature. Nevertheless, results from the simulation are useful for the determination of the microheater dimensions and could not be changed in practice. The heat distribution of the sensor chip under an applied power of 165 mW is shown in Fig. 1(a). The microheater and electrodes were patterned using conventional photolithography, sputter deposition and lift−off processes [30]. Five layers, namely Cr (10 nm), Pt (30 nm), Au (10 nm), Pt (50 nm) and ITO (20 nm), were sputter deposited on a fused silica substrate (which had an annealing point of 1200 °C) to provide the thin film with a sandwich structure from the bottom to the top.

2.2. Growth of SnO_2 nanowires through chemical vapor deposition method

After electrode fabrication, the sensor chip was loaded in a chemical vapor deposition (CVD) system for the growth of SnO_2 nanowires, as reported in [30]. In a typical procedure, 0.3 g Sn powder was loaded in an alumina boat. The sensor chip was then placed upside down on the top of the alumina boat. The boat with the sensor chip was positioned at the centre of a CVD tube furnace for nanowire growth. After flushing with Ar gas to clean the tube and vacuum pumping down to 1.5×10^{-1} mTorr, the furnace

temperature was increased to the reaction temperature of 750 °C for a period of 20 min. An O_2 gas flow of 0.5 sccm was then introduced into the tube during the 20 min reaction. Finally, the furnace was naturally cooled down to room temperature. As seen in the thin film sandwich structure, the ITO layer on the top prevented the SnO_2 nanowires from growing on the other surface of the Pt layer. The Au catalyst layer within the sandwich promoted the SnO_2 nanowires due to the vapour—liquid—solid (VLS) growth mechanism. Thus, the ITO and Au layers positions forced the SnO_2 nanowires to grow from the sandwich structure. The synthesized materials were studied by field emission scanning microscopy (SEM, JEOL 7600F) and high resolution transmission electron microscopy (HRTEM, JEM2100). Fig. 1(b) shows the centre part of a fabricated sensor chip.

2.3. Sensor characterization

Fig. 2 shows the measurement setup with all in-house developed systems with the exception of the Arduino Mega 2560 board, which is based on an ATMega 2560 chip. In most studies, the sensing elements (or sensors) are located in the vicinity of the microheater, and two electrodes are needed for the resistance measurement of each sensor [31]. Therefore, sensor heating occurs indirectly, and the heat transfer depends on the distance between the microheater and the sensing elements, the thermal conductivity of the substrate, and the conditions for thermal convection and irradiation. This work used a design to circumvent these problems. Here, the sensors are bridging the microheater and their electrodes, enabling direct heating of the sensor, and thus saving power consumption. Each sensor needs only one electrode of its own, with the second one serving as the source pad of the microheater. Fig. 2(a) shows that the design is much simpler than the above-mentioned design, considering that a voltage can be applied to the sensor heater at the same time as its resistance is registered. The sensor chip was mounted on a printed circuit board (PCB) for easy handling. A programmable voltage source was connected to the microheater to power the sensor. Each sensor (S1, S2, S3 and S4) was connected in series with a digital resistor (100 kΩ). The output signals from sensors S1, S2, S3 and S4 are V1, V2, V3 and V4, respectively. The dynamic voltage changes from the four sensors are collected by the data acquisition system and used to calculate the sensor responses. To increase the accuracy of the signals, we equipped the acquisition system with an external ultra-small and low-power Analog-to-Digital converter (ADS1115, Texas Instruments), which provided 16-bit precision with a sampling rate of 860 samples/s over the inter-integrated circuit (I^2C) interface. The entire system (Arduino module, external ADCs and PC) and the signal processing were controlled by an in-house developed software in Labview Environment (National Instruments). Fig. 2(b) and (c) show the photos of the main board and the user interface of the software for data acquisition.

During gas-sensing measurements, the voltage drop across the series resistors was measured continuously, while the atmosphere (in the plastic box, Fig. 2(b)) was switched back and forth from air to target gas. In this study, the test gases were ethanol, methanol, acetone, isopropyl alcohol (IPA), hydrogen and ammonia. By using this setup and the developed software, signals from the four sensors S1, S2, S3 and S4 could be measured simultaneously for gas ON duration of 150 s and gas OFF duration of 250 s. The sensor response was defined as V/V_{air}, where V and V_{air} were the voltage drop measured across the reference resistor in target gas ambient and in air (which was considered as the background signal).
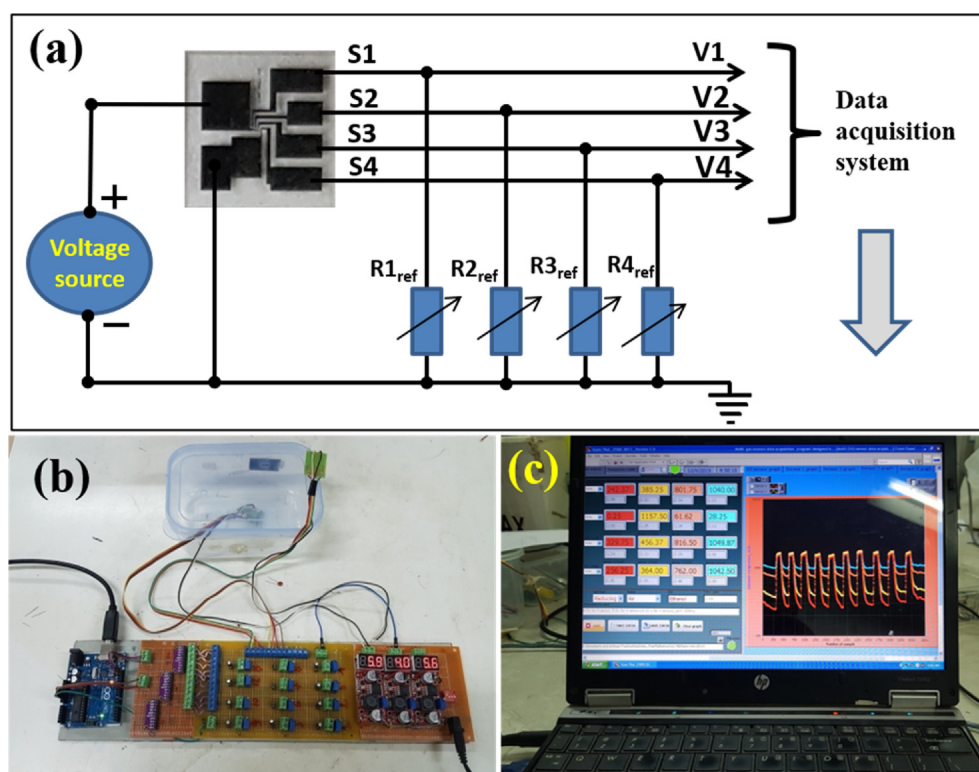

Fig. 2. Electronic connection of sensor chip (a); electronic circuit board (b); and PC software (c) for data acquisition.

3. Results and discussion

Fig. 3 shows a collage of pictures of the experimental results. Fig. 3(a) shows a sensor chip and a board made from a PCB laminate for mounting and protection of the sensor chip. The sensor was mounted on the board using conductive glue. Thus, the analytical gases come into contact with the sensors through the hole in the board. Fig. 3(b) shows the thermal distribution on the sensor chip captured by an infrared camera (FLIR, ThermoVision A40), where the power consumed by the microheater was 165 mW, confirming that the maximum temperature was 450 °C. The temperatures of sensors S1, S2, S3 and S4 were approximately 450, 325, 250 and 210 °C, respectively, covering the desired working temperatures for

this experiment. The SEM image of the sensor chip shown in Fig. 3(c) displays the microheater, sensor electrodes and SnO_2 nanowires at the edges. The gaps between sensor electrodes and heater were approximately 10 μm. The SEM image at high magnification in Fig. 3(d) shows that the nanowires make a relatively dense but highly porous mat of entangled nanowires. The porosity is important to allow the quick diffusion of analytic gases to the sensing nanowires [32]. Very long SnO_2 nanowires were obtained, with sizes reaching hundreds of micrometres, which bridged the gap between the electrodes and the microheater. During CVD growth, Au acted as a catalyst for the VLS growth mechanism. Considering that the Au catalyst layer was sandwiched between two Pt layers, only the edges of the Au layer were exposed to Sn
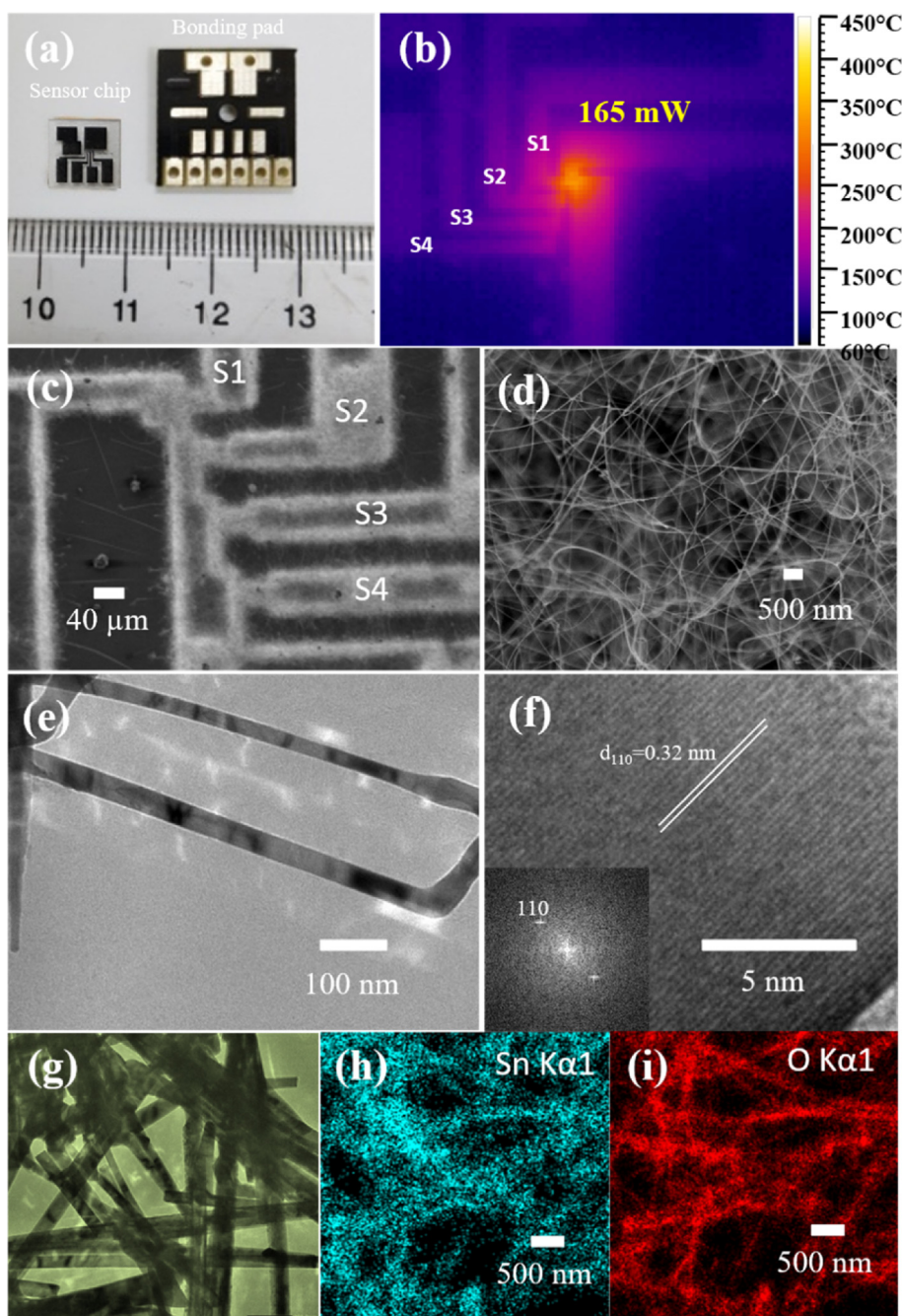
Fig. 3. Picture of the sensor chip and its mounting board (a); IR emission image at applied power of 165 mW (b); low and high magnification SEM image (c, d) of the fabricated sensor; TEM and HRTEM images (e, f); STEM image (g); and EDS mapping of SnO_2 nanowires (h, i).
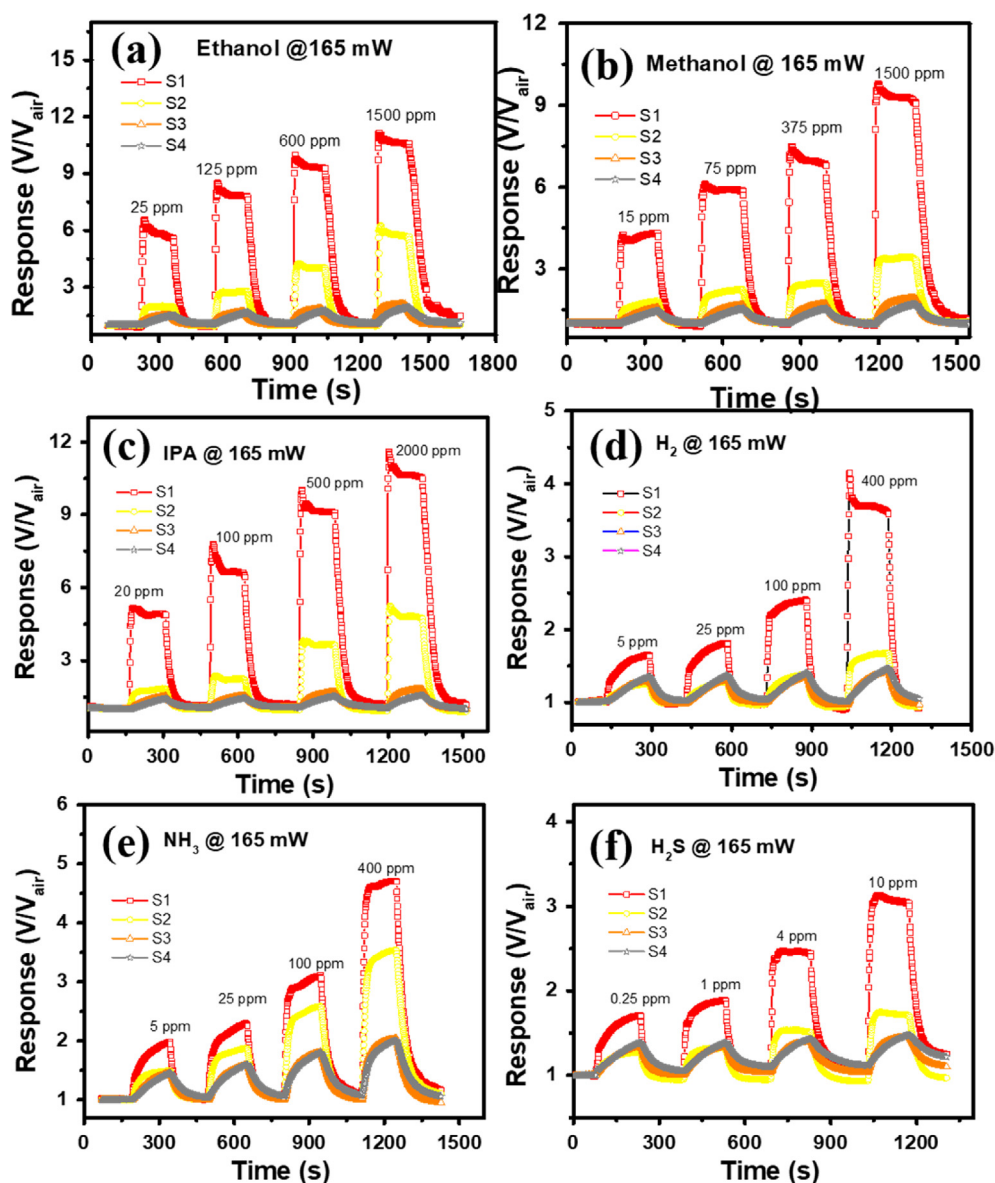
Fig. 4. Transient response of sensor array to different gases at power supply of 165 mW: ethanol (a), methanol (b), IPA (c), H$_2$ (d), NH$_3$ (e) and H$_2$S (f). Note: Red, yellow, brown and grey lines represent the sensing characteristics of sensor S1, S2, S3 and S4, respectively.

vapour and promoted the growth of SnO$_2$ nanowire. The gap between the two electrodes is important for determining the diameter of the on-chip nanowire growth and, thus, the sensor's sensitivity. Upon initial growth, the diameter of the nanowires was very large, but it subsequently decreased [30]. Thus, the aforementioned gaps should be sufficiently large to achieve the small nanowires desired before they make contact with one another. As shown in the SEM image in Fig. 3(d) and in the TEM image in Fig. 3(e), homogenous nanowires with an ultrafine diameter of approximately 50 nm could be obtained after prolonging of growth time. The nanowires have a very smooth and clean surface, as is the nature of single-crystal nanowire. Highly crystalline nanowires were used to ensure the good stability of the sensor.

The HRTEM image of a nanowire is shown in Fig. 3(f), displaying clear lattice fringes with a gap of 0.32 nm, corresponding to the interspace of the (110) planes of tetragonal SnO$_2$. The inset of Fig. 3(f) shows the fast Fourier transform (FFT) of the corresponding HRTEM, confirming the high crystallinity of the synthesized SnO$_2$

nanowires. Fig. 3(g) shows the STEM image of the sample used for EDS mapping. The composition and distribution of elements in the sample were characterized by EDS mapping, as shown in Fig. 3(h) and (i). Oxygen and tin atoms were homogenously distributed all over the SnO$_2$ nanowires.

The gas sensing characteristics of the fabricated sensor array were tested against ethanol, methanol, IPA, H$_2$, NH$_3$ and H$_2$S at different concentrations, at an applied power of 165 mW. The transient response versus time of sensors S1, S2, S3 and S4 were continuously recorded, as shown in Fig. 4. The ethanol sensing characteristics shown in Fig. 4(a) confirm that the sensor S1 has the highest response value, followed by S2, S3 and S4, because of the decrease in temperature from sensor S1 to S4. The sensors showed a similar trend in response when tested against the other reducing gases, as shown in Fig. 4(b)–(f). Considering that the sensor array used one sensing material, SnO$_2$, the temperature gradient from sensors S1 to S4 could result in different sensing characteristics for different gases. Three factors determine the sensing characteristics
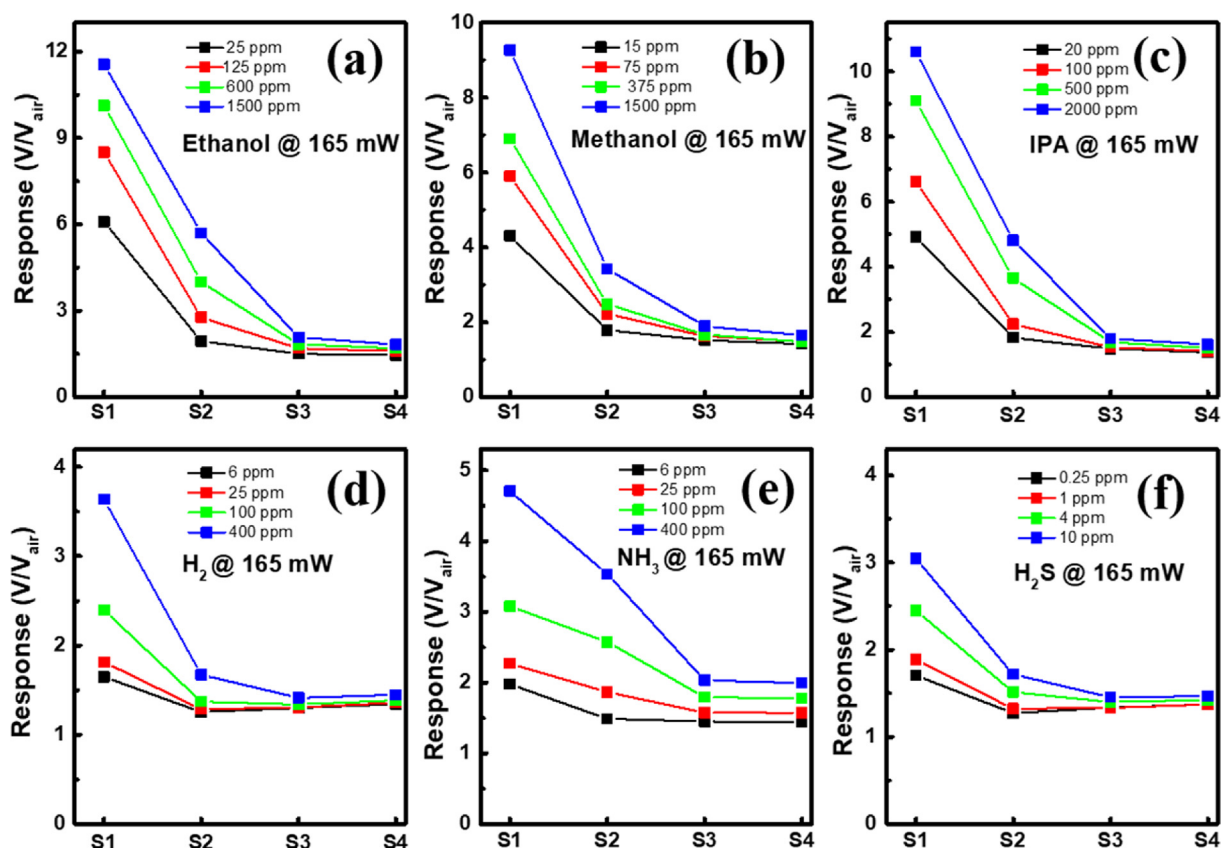
Fig. 5. Response plot of sensor array to different gases at a supplied power of 165 mW: ethanol (a), methanol (b), IPA (c), H_2 (d), NH_3 (e) and H_2S (f).

of the sensor array, namely, response values, response speeds, and trends (rates) in the variation of response with temperatures and various gases. Sensor S1 had the highest response values of 6.1, 8.56, 10.1 and 11.6 for 25, 125, 600 and 1500 ppm ethanol, respectively. However, sensor S4 had very low response values of 1.45, 1.59, 1.69 and 1.8 for 25, 125, 600 and 1500 ppm ethanol, respectively. A similar trend was found for other gases, such as methanol, IPA, H_2, NH_3 and H_2S.

Fig. 5 shows the plots of the sensor response against different test gases at four different concentrations versus their operation temperatures (in the form of sensor S1–S4 in the field of temperature gradient). The decreasing trends are clearly similar, regardless of the test gas. However, the reduction in rate of response differs for each gas. The response values to 25 ppm ethanol were 6.1, 1.9, 1.49 and 1.45 for sensors S1, S2, S3 and S4, respectively. The reduction in rate of response to VOC gases from sensor S1 to sensor S4 is faster than that to H_2, NH_3 and H_2S. For a given sensor, the response values to different gases also differs, thereby enabling the use of such data for gas classification.

In addition to the response values, the response speeds are also important in gas sensor application. Table 1 shows the response and recovery times of different sensors for ethanol. For a given ethanol concentration, the response and recovery times increases from sensor S1 to sensor S4. This was also a result of the temperature gradient in the sensor array. Sensor S1 has the fastest response times of 15, 9, 5 and 3 s for 25, 125, 600 and 1500 ppm ethanol, respectively. In contrast to response time, the recovery time of sensor S1 increases from 41 to 101 with an increment of ethanol concentration from 5 ppm to 1500 ppm. Sensor S1 gave the best performance to ethanol, with the highest response value and the fastest response and recovery times.

Table 2 shows the response and recovery times of different sensors for 600 ppm ethanol, 375 ppm methanol, 500 ppm IPA, 400 ppm H_2, 400 ppm NH_3 and 4 ppm H_2S. Sensor S1 showed the fastest response and recovery time to almost all gases tested, followed by sensors S2, S3 and S4. For sensor S1, the fastest response time was 3 s–500 ppm IPA, and the slowest response time was 17 s to 4 ppm H_2S. This result revealed that for a given working temperature, the response speeds of SnO$_2$ nanowires are different for

Table 1
Response and recovery times of sensor array to ethanol gas.

Ethanol	Response time (s)				Recovery time (s)			
	S1	S2	S3	S4	S1	S2	S3	S4
25 ppm	15	18	98	130	41	48	91	105
125 ppm	9	17	96	125	58	62	107	128
600 ppm	5	11	80	110	82	93	123	164
1500 ppm	3	6	52	100	101	112	135	213

Table 2
Response and recovery times of sensor array to 600 ppm ethanol, 375 ppm methanol, 500 ppm IPA, 400 ppm H_2, 400 ppm NH_3 and 4 ppm H_2S.

Gas	Response time (s)				Recovery time (s)			
	S1	S2	S3	S4	S1	S2	S3	S4
600 ppm Ethanol	5	11	80	110	82	70	123	164
375 ppm Methanol	4	29	96	118	57	82	156	191
500 ppm IPA	3	39	103	116	53	63	145	184
400 ppm H_2	9	11	29	35	91	72	108	113
400 ppm NH_3	14	24	36	43	150	180	197	225
4 ppm H_2S	17	30	81	107	95	116	164	187
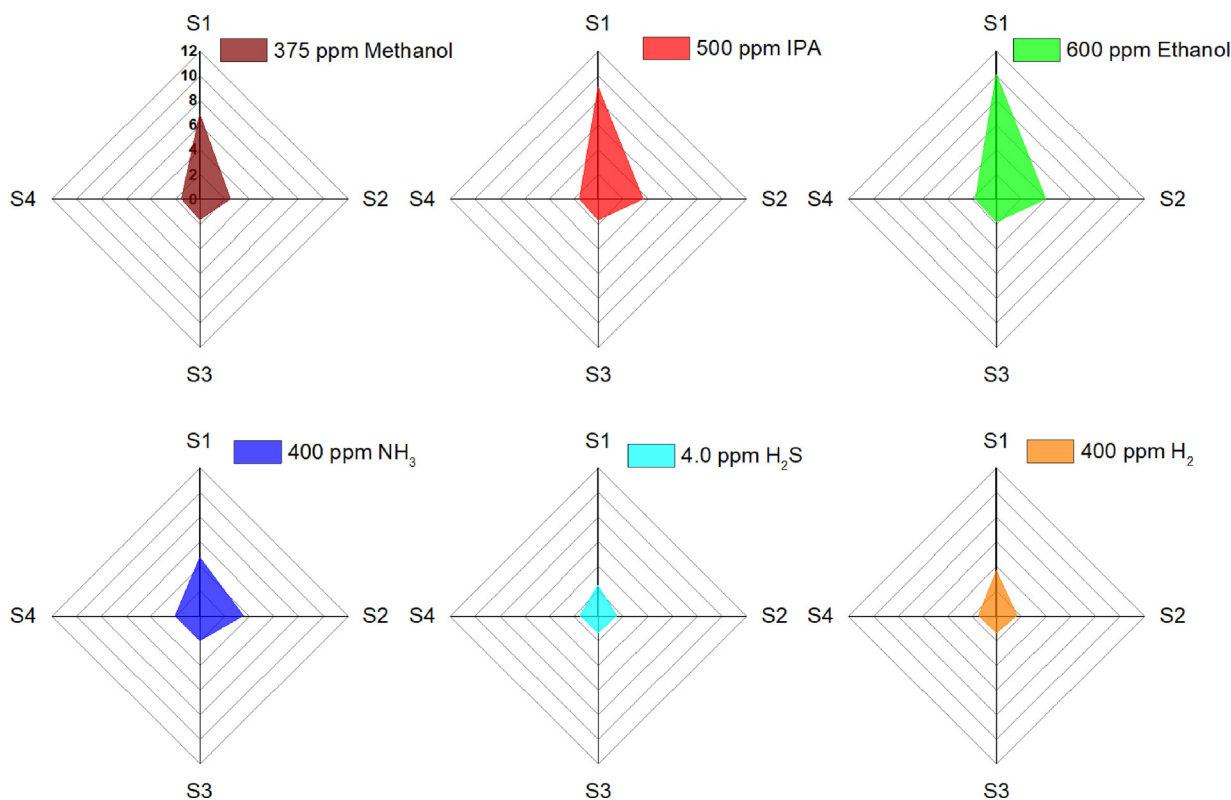
Fig. 6. Classification of various gases (methanol, IPA, ethanol, NH_3, H_2S and H_2) by using radar plots from a single device.

each gas. For the recovery time, sensor S1 showed the shortest time of 53 s—500 ppm IPA and the longest time of 150 s—400 ppm NH_3.

For vision classification of different gases, we presented the four sensor responses to 375 ppm Methanol, 500 ppm IPA, 600 ppm Ethanol, 400 ppm NH_3, 400 ppm H_2 and 4 ppm H_2S in radar plots. The results are shown in Fig. 6 with the sensors (S1, S2, S3 and S4) as the four dimensions and the gas response as the amplitude. It can be seen that the shape and size of plots differed for each gas, especially for VOC (ethanol, IPA and methanol), NH_3 and H_2S. While the plot area was proportional to the gas concentration, its shape seemed typical for each gas. Notably, each radar plot contains four directions instead of only one if using single resistive sensor output. For more detail, we could see the similar shapes of methanol, iso-propanol and ethanol responses. This would come from the alcohol functional group of the three gases. A stronger classification, such as Principle Component Analysis (PCA) or Support Vector Machine (SVM) PCA or SVM, would bring a better result in this case. With this simple vision expression, it was possible to recognise NH_3, H_2S and H_2 gases from the alcohol group by the human eye. Hence, the variation in working temperature in sensors S1—S4 is sufficient to classify methanol, IPA, ethanol, NH_3, H_2S and H_2 gases with an integrated single-material chip.

4. Conclusion

We introduced an effective design and simple fabrication of an edge-grown SnO_2 nanowire-based sensor array for the real-time monitoring and classification of multiple gases. The microheater and electrodes were fabricated simultaneously in the same lithography, sputter deposition and lift—off processes. The sandwich of thin films of Cr/Pt/Au/Pt/ITO (bottom to top) was used to pattern the chip on a fused silica substrate, and was capable of forcing SnO_2 to grow from the edges of the microheater and the electrodes. The sensor array was investigated for sensing performance and classification of six different gases (methanol, IPA, ethanol, NH_3, H_2S and H_2). A temperature gradient, evaluated from 210 °C to 450 °C, was realized using a microheater with varying resistance along its length to allow the directly-heated sensors to work at different temperatures. The edge-grown nanowire sensor array of single sensing material operated well as effective multiple sensors.

Declaration of Competing Interest

The authors have no conflict of interests to declare regarding the publication of this paper.

Acknowledgments

References

[1] D.H. Kim, T.H. Kim, W. Sohn, J.M. Suh, Y.-S. Shim, K.C. Kwon, K. Hong, S. Choi, H.-G. Byun, J.-H. Lee, H.W. Jang, Au decoration of vertical hematite nanotube arrays for further selective detection of acetone in exhaled breath, Sensor. Actuator. B Chem. 274 (2018) 587—594, https://doi.org/10.1016/j.snb.2018.07.159.

[2] J.D. Pleil, K.K. Isaacs, High-resolution mass spectrometry: basic principles for using exact mass and mass defect for discovery analysis of organic molecules in blood, breath, urine and environmental media, J. Breath Res. 10 (2016) 12001, https://doi.org/10.1088/1752-7155/10/1/012001.

[3] N.X. Thai, N. Van Duy, N. Van Toan, C.M. Hung, N. Van Hieu, N.D. Hoa, Effective monitoring and classification of hydrogen and ammonia gases with a bilayer Pt/SnO2 thin film sensor, Int. J. Hydrogen Energy 45 (2020) 2418—2428, https://doi.org/10.1016/j.ijhydene.2019.11.072.

[4] P.G. Choi, N. Izu, N. Shirahata, Y. Masuda, SnO 2 nanosheets for selective alkene gas sensing, ACS Appl. Nano Mater. 2 (2019) 1820—1827, https://doi.org/10.1021/acsanm.8b01945.

[5] A. Kolmakov, M. Moskovits, Chemical sensing and catalysis by one-dimensional metal-oxide nanostructures, Annu. Rev. Mater. Res. 34 (2004) 151–180, https://doi.org/10.1146/annurev.matsci.34.040203.112141.

[6] A. Ponzoni, C. Baratto, N. Cattabiani, M. Falasconi, V. Galstyan, E. Nunez-Carmona, F. Rigoni, V. Sberveglieri, G. Zambotti, D. Zappa, Metal oxide gas sensors, a survey of selectivity issues addressed at the SENSOR lab, Brescia (Italy), Sensors 17 (2017) 714, https://doi.org/10.3390/s17040714.

[7] A.M. Kummer, A. Hierlemann, H. Baltes, Tuning sensitivity and selectivity of complementary metal oxide semiconductor-based capacitive chemical microsensors, Anal. Chem. 76 (2004) 2470–2477, https://doi.org/10.1021/ac0352272.

[8] M. Kumar, V.S. Bhati, S. Ranwa, J. Singh, M. Kumar, Pd/ZnO nanorods based sensor for highly selective detection of extremely low concentration hydrogen, Sci. Rep. 7 (2017) 1–9, https://doi.org/10.1038/s41598-017-00362-x.

[9] P.E. Keller, L.J. Kangas, L.H. Liden, S. Hashem, R.T. Kouzes, Electronic noses and their applications, in: IEEE Tech. Appl. Conf. Work. Northcon/95. Conf. Rec, IEEE, 1995, pp. 116–119, https://doi.org/10.1109/NORTHC.1995.485024.

[10] H.-G. Byun, J.-B. Yu, C.-Y. Kang, B.K. Jang, H.-R. Lee, Comparative analysis between blood test and breath analysis using sensors array for diabetic patients, Proceedings 14 (2019) 22, https://doi.org/10.3390/proceedings2019014022.

[11] S.I. Hwang, N.G. Franconi, M.A. Rothfuss, K.N. Bocan, L. Bian, D.L. White, S.C. Burkert, R.W. Euler, B.J. Sopher, M.L. Vinay, E. Sejdic, A. Star, Tetrahydrocannabinol detection using semiconductor-enriched single-walled carbon nanotube chemiresistors, ACS Sens. 4 (2019) 2084–2093, https://doi.org/10.1021/acssensors.9b00762.

[12] B. Wang, J.C. Cancilla, J.S. Torrecilla, H. Haick, Artificial sensing intelligence with silicon nanowires for ultraselective detection in the gas phase, Nano Lett. 14 (2014) 933–938, https://doi.org/10.1021/nl404335p.

[13] H.S. Kim, T. Lee, Pattern Recognition for Selective Odor Detection with Gas Sensor Arrays, 2012, pp. 16262–16273, https://doi.org/10.3390/s121216262.

[14] S. Ghosh, A. Roy, S. Singh, Sensor Array for Manhole Gas Analysis, 2012, https://doi.org/10.1109/ISPTS.2012.6260863.

[15] Y. Zhang, J. Zhao, T. Du, Z. Zhu, J. Zhang, Q. Liu, OPEN A gas sensor array for the simultaneous detection of multiple VOCs, Sci. Rep. (2017) 1–8, https://doi.org/10.1038/s41598-017-02150-z.

[16] Y.S. Zhang, J. Aleman, S.R. Shin, T. Kilic, D. Kim, S.A. Mousavi Shaegh, S. Massa, R. Riahi, S. Chae, N. Hu, H. Avci, W. Zhang, A. Silvestri, A. Sanati Nezhad, A. Manbohi, F. De Ferrari, A. Polini, G. Calzone, N. Shaikh, P. Alerasool, E. Budina, J. Kang, N. Bhise, J. Ribas, A. Pourmand, A. Skardal, T. Shupe, C.E. Bishop, M.R. Dokmeci, A. Atala, A. Khademhosseini, Multisensor-integrated organs-on-chips platform for automated and continual in situ monitoring of organoid behaviors, Proc. Natl. Acad. Sci. Unit. States Am. 114 (12) (2017) E2293–E2302, https://doi.org/10.1073/pnas.1612906114.

[17] K.J. Albert, N.S. Lewis, C.L. Schauer, G.A. Sotzing, S.E. Stitzel, T.P. Vaid, D.R. Walt, Cross-reactive chemical sensor arrays, Chem. Rev. 100 (2000) 2595–2626, https://doi.org/10.1021/cr980102w.

[18] H.V. Shurmer, J.W. Gardner, P. Corcoran, Intelligent vapour discrimination using a composite 12-element sensor array, Sensor. Actuator. B Chem. 1 (1990) 256–260, https://doi.org/10.1016/0925-4005(90)80211-H.

[19] H.M. Fahad, H. Shiraki, M. Amani, C. Zhang, V.S. Hebbar, W. Gao, H. Ota, M. Hettick, D. Kiriya, Y.-Z. Chen, Y.-L. Chueh, A. Javey, Room temperature multiplexed gas sensing using chemical-sensitive 3.5-nm-thin silicon transistors, Sci. Adv. 3 (2017), e1602557, https://doi.org/10.1126/sciadv.1602557.

[20] D. Lee, H. Jung, J. Lim, M. Lee, S. Ban, SnO2 Gas Sensing Array for Combustible and Explosive Gas Leakage Explosive Gas Recognition System Using Thick ® Lm Sensor Array and Neural Network, 2002, https://doi.org/10.1109/JSEN.2002.800685.

[21] W. Shin, T.G. Id, D. Nagai, T. Itoh, A. Tsuruta, Thermoelectric Array Sensors with Selective, 2018, pp. 1–10, https://doi.org/10.3390/s18051579.

[22] P. Lorwongtragool, E. Sowade, N. Watthanawisuth, R.R. Baumann, T. Kerdcharoen, A novel wearable electronic nose for healthcare based on flexible printed chemical sensor array, Sensors 14 (2014) 19700–19712, https://doi.org/10.3390/s141019700.

[23] V.V. Sysoev, I. Kiselev, M. Frietsch, J. Goschnick, Temperature gradient effect on gas discrimination power of a metal-oxide thin-film sensor microarray, Sensors 4 (2004) 37–46, https://doi.org/10.3390/s40400037.

[24] L. Francioso, A. Forleo, A.M. Taurino, P. Siciliano, L. Lorenzelli, V. Guarnieri, A. Adami, G. Agnusdei, Sens. Actuators B: Chem. Linear Temp. Microhotplate Gas Sens. Array Automotive Cabin Air Quality Monitoring 134 (2008) 660–665, https://doi.org/10.1016/j.snb.2008.06.008.

[25] M. Tonezzer, D.T.T. Le, S. Iannotta, N. Van Hieu, Selective discrimination of hazardous gases using one single metal oxide resistive sensor, Sensor. Actuator. B Chem. 277 (2018) 121–128, https://doi.org/10.1016/j.snb.2018.08.103.

[26] M. Tonezzer, J.-H. Kim, J.-H. Lee, S. Iannotta, S.S. Kim, Predictive gas sensor based on thermal fingerprints from Pt-SnO2 nanowires, Sensor. Actuator. B Chem. 281 (2019) 670–678, https://doi.org/10.1016/j.snb.2018.10.102.

[27] M.S. Wiederoder, E.C. Nallon, M. Weiss, S.K. McGraw, V.P. Schnee, C.J. Bright, M.P. Polcha, R. Paffenroth, J.R. Uzarski, Graphene nanoplatelet-polymer chemiresistive sensor arrays for the detection and discrimination of chemical warfare agent simulants, ACS Sens. 2 (2017) 1669–1678, https://doi.org/10.1021/acssensors.7b00550.

[28] V.V. Sysoev, J. Goschnick, T. Schneider, E. Strelcov, A. Kolmakov, A gradient microarray electronic nose based on percolating SnO2 nanowire sensing elements, Nano Lett. 7 (2007) 3182–3188, https://doi.org/10.1021/nl071815+.

[29] C. Arnold, D. Haeringer, I. Kiselev, J. Goschnick, Sub-surface probe module equipped with the Karlsruhe Micronose KAMINA using a hierarchical LDA for the recognition of volatile soil pollutants, Sensor. Actuator. B Chem. 116 (2006) 90–94, https://doi.org/10.1016/j.snb.2005.12.068.

[30] T.M. Ngoc, N. Van Duy, N. Duc Hoa, C. Manh Hung, H. Nguyen, N. Van Hieu, Effective design and fabrication of low-power-consumption self-heated SnO2 nanowire sensors for reducing gases, Sensor. Actuator. B Chem. 295 (2019) 144–152, https://doi.org/10.1016/j.snb.2019.05.074.

[31] E.N. Dattoli, A.V. Davydov, K.D. Benkstein, Tin oxide nanowire sensor with integrated temperature and gate control for multi-gas recognition, Nanoscale 4 (2012) 1760, https://doi.org/10.1039/c2nr11885h.

[32] N.D. Hoa, N. Van Quy, Y. Cho, D. Kim, Porous single-wall carbon nanotube films formed by in Situ arc-discharge deposition for gas sensors application, Sensor. Actuator. B Chem. 135 (2009) 656–663, https://doi.org/10.1016/j.snb.2008.10.041.